TrkB is necessary for pruning at the climbing fibre–Purkinje cell synapse in the developing murine cerebellum

Erin M. Johnson, Ethan T. Craig and Hermes H. Yeh

Department of Physiology, Dartmouth Medical School, Lebanon, NH 03756, USA

TrkB, the cognate receptor for brain-derived neurotrophic factor and neurotrophin-4, has been implicated in regulating synapse formation in the central nervous system. Here we asked whether TrkB plays a role in the maturation of the climbing fibre–Purkinje cell (CF–PC) synapse. In rodent cerebellum, Purkinje cells are initially innervated by multiple climbing fibres that are subsequently culled to assume the mature mono-innervated state, and whose contacts translocate from the soma to the dendrites. By employing transgenic mice hypomorphic or null for TrkB expression, our results indicated that perturbation of TrkB in the immature cerebellum resulted in ataxia, that Purkinje cells remained multiply innervated by climbing fibres beyond the normal developmental time frame, and that synaptic transmission at the parallel fibre–Purkinje cell synapse remained functionally unaltered. Mechanistically, we present evidence that attributes the persistence of multiple climbing fibre innervation to an obscured discrimination of relative strengths among competing climbing fibres. Soma-to-dendrite translocation of climbing fibre terminals was unaffected. Thus, TrkB regulates pruning but not translocation of nascent CF–PC synaptic contacts.

(Resubmitted 28 March 2007; accepted after revision 20 April 2007; first published online 26 April 2007)
Corresponding author Hermes H. Yeh: Department of Physiology, Dartmouth Medical School, One Medical Center Drive, Lebanon, NH 03756, USA. Email: hermes.yeh@dartmouth.edu

The pruning of supernumerary contacts is a fundamental process in synaptogenesis. This process has been studied extensively at the neuromuscular junction, where neurotrophins have been implicated in regulating synaptic pruning (Sanes and Lichtman, 1999). In the central nervous system (CNS), synaptic pruning occurs in the developing cerebellum at nascent climbing fibre–Purkinje cell (CF–PC) synapses, hallmarked by the culling of multiple climbing fibres that initially innervate individual immature Purkinje cells. However, whether neurotrophins regulate synaptic pruning in the CNS is unknown. Neurotrophins, notably brain-derived neurotrophic factor (BDNF) signalling via TrkB, have been reported to regulate other components of synaptogenesis, such as synaptic connectivity and density (Cabelli *et al.* 1997; Causing *et al.* 1997; Hu *et al.* 2005; Lush *et al.* 2005).

Neuroanatomical studies indicate that climbing fibres innervate Purkinje cells as early as embryonic day 19 (Morara *et al.* 2001), and early electrophysiological studies have established that immature stimulus-evoked climbing fibre responses can be detected in Purkinje cells by postnatal day (P)2–3 (Crepel, 1971; Puro & Woodward, 1977; Mariani & Changeux, 1981). These and more recent studies have revealed that multiple climbing fibres innervate most Purkinje cells at this early postnatal stage of cerebellar development (Hashimoto & Kano, 2003; Scelfo & Strata, 2005). Beyond the first postnatal week, pruning occurs at the CF–PC synapse such that, by the end of the third postnatal week, individual Purkinje cells are predominantly innervated by a single climbing fibre (Hashimoto & Kano, 2003, 2005; Nishiyama & Linden, 2004). Perturbation of the pruning process at the developing CF–PC synapse is associated with impaired motor coordination (Kashiwabuchi *et al.* 1995; Offermanns *et al.* 1997; Kano *et al.* 1998; Ribar *et al.* 2000; Ichise *et al.* 2000; Hashimoto *et al.* 2001). Both may be linked to compromised BDNF signalling (Riva-Depaty *et al.* 1998). In this light, BDNF knockout and TrkB conditional knockout mice are ataxic (Schwartz *et al.* 1997; Rico *et al.* 2002), but the disposition of Purkinje cell innervation by climbing fibres under conditions of diminished TrkB signalling in the developing cerebellum has not been investigated.

In the developing and adult cerebellar cortex, Purkinje cells, basket/stellate cells, Golgi cells, and differentiated granule cells express TrkB (Ringstedt *et al.* 1993; Gao *et al.* 1995; Dieni & Rees, 2002). TrkB candidate ligands, BDNF and neurotrophin-4 (NT-4), are also present (Timmusk *et al.* 1993; Castren *et al.* 1995; Li *et al.* 2001; Dieni & Rees, 2002). These findings provide the neuroanatomical substrate for BDNF–TrkB interaction in the cerebellar cortex, and allow for testing the hypothesis that TrkB

 DOI: 10.1113/jphysiol.2007.133561

plays a role in regulating the maturation of the CF–PC synapse.

Here we asked whether disruption of TrkB signalling alters the pruning of contacts that are initially formed at the developing CF–PC synapse. We report that transgenic mice, hypomorphic or conditionally null for TrkB expression in the cerebellum, are ataxic and that this is tightly correlated with a persistence of multiple climbing fibre innervation of cerebellar Purkinje cells.

Methods

All procedures involving animals were carried out in accordance with the NIH Guide for the Care and Use of Laboratory Animals, and were approved by Institutional Animal Care and Use Committee at Dartmouth Medical Center. Animals were killed by CO_2 inhalation.

Transgenic mouse strains

The transgenic mouse line *fBZ/fBZ* with hypomorphic expression of TrkB was provided by Dr Louis Reichardt (University of California, San Francisco, CA, USA). These mice were created by flanking TrkB cDNA with two loxP elements (*fBZ* allele). Mice harbouring two such alleles display hypomorphic expression of TrkB (Xu *et al.* 2000). To create a conditional knockout of TrkB, mice harbouring the *fBZ* allele were crossed with mice in which *wnt1* drives Cre recombinase (*Wnt1Cre* mouse line; Jackson Laboratory, Bar Harbour, ME, USA). Recombination occurs at embryonic day 8.5 and results in TrkB deletion throughout most of the hindbrain, including the cerebellum (Danielian *et al.* 1998; Rico *et al.* 2002). Data derived from mice positive for the *cre* allele but without an *fBZ* allele were included with the wild-type mice since there were no differences between the *cre*-positive and -negative mice on any of the parameters examined in the present study.

Immunohistochemistry

Cerebella were removed and immerse-fixed overnight in 4% paraformaldehyde. Cryosections (20 μm) were obtained using a sliding microtome and stored in PBS (pH 7.4). Sections were incubated at room temperature for 30 min in blocking solution consisting of 10% normal goat serum (NGS) in 0.1 M PBS and 0.5% Triton X-100. All subsequent reactions were carried out in 0.1 M PBS containing 1% NGS and 0.5% Triton X-100. The primary antibodies used were calbindin (1:2000; Sigma, St Louis, MO, USA), TrkB (1:500; Santa Cruz Biotechnology, Santa Cruz, CA, USA), VGluT1 (1:1000; provided by Dr Robert Edwards, University of California, San Francisco), and VGluT2 (1:1000; provided by Dr Masahiko Watanabe, Hokkaido University, Sapporo, Japan). Double and triple immunohistochemical labelling was accomplished by overnight incubation at 4°C with the primary antibodies, followed by a 2 h incubation at room temperature with Alexa-dye-conjugated secondary antibodies (1:850, goat anti-rabbit, -mouse, or -guinea pig; Molecular Probes, Eugene, OR, USA). The sections were then washed, mounted, and coverslipped. Immunofluorescent images were captured using a laser-scanning confocal microscope (FV300; Olympus, Melville, NY, USA) with a ×60 oil objective (aperture: 1.4), and edited using Photoshop 6.0 (Adobe Systems, Inc., San Jose, CA, USA). Immunoreactive puncta were counted using ImageJ software (National Institutes of Health). Data are expressed as means ± standard error of the mean (S.E.M.), and analysis was done using a one-way ANOVA or a χ^2 test. At least three sections per mouse from three mice of each genotype were analysed.

Protein assay and ELISA

Cerebella were lysed in buffer containing (mM) 137 NaCl, 20 Tris-HCl (pH 7.6), 1% Nonidet P40, 10% glycerol, 1 PMSF, 0.5 sodium orthovanadate, and 1% protease inhibitor cocktail (Sigma). Total protein in the cerebellar extracts was then measured using the DC protein Assay (Bio-Rad, Hercules, CA, USA). Levels of BDNF were assessed from the same whole cerebellar extracts using the BDNF Emax ImmunoAssay System (Promega, Madison, WI, USA). Data are expressed as means ± S.E.M. Statistical analysis was performed using one-way ANOVA.

Western blot analysis

Cerebella were lysed in Tris-buffered saline (TBS) containing (mM) 10 Tris (pH 7.6), 50 NaCl, 30 sodium tetraphosphate, 50 sodium fluoride, 1 sodium orthovanadate, 0.1% SDS, 1% protease inhibitor cocktail (Sigma), and 2% Nonidet P40. Samples were rocked for 30 min at 4°C and then centrifuged at 10 000 *g* for 30 min at 4°C. Supernatants were boiled in sample buffer containing 62.5 mM Tris buffer (pH 6.8), 2% SDS, 10% glycerol, 1% Bromophenol blue, and 2.5% betamercaptoethanol for 5 min and then analysed by SDS-PAGE. After electrophoresis, proteins were transferred to 0.45 μm nitrocellulose membrane for 30 min at 13 mV. Membranes were then washed in TBS-T (TBS + 0.5% Tween) 3 × 10 min. After washing, membranes were blocked for 2 h at room temperature in 5% non-fat dry milk in TBS-T and then incubated overnight in primary antibody at 4°C. Blots were probed with primary antibody against either TrkB (1:500; Santa Cruz Biotechnology) or βIII-tubulin (1:40 000; Promega). Blots were then washed 5 × 10 min in TBS-T and

incubated for 1 h in horseradish-peroxidase-conjugated, goat anti-rabbit or -mouse secondary antibody (1:2000; Molecular Probes). Proteins were detected using ECL (Perkin Elmer Life Sciences, Boston, MA, USA) and chemiluminescence film (Kodak, Rochester, NY, USA). Blots were quantified by densitometry with AlphaEase FC version 3.1.2 (Alpha Innotech, San Leandro, CA, USA). Densitometry values of TrkB expression were normalized to densitometry values for βIII-tubulin expression of the same sample. Data were then normalized and expressed as a percentage of TrkB expression in whole brain extract. Aliquots of the same whole brain extract were used for each blot. Statistical analysis was performed using one-way ANOVA.

Behavioural testing

Ataxia was assessed using a combination of footprint and rotarod tests. Abnormalities in gait were assessed at P20–24 using a footprint assay. A footprint pattern was obtained by applying non-toxic paint to the forepaws and the hindpaws of a mouse. As a routine, the forepaws were painted orange and the hindpaws were painted blue. The subject then walked through a tunnel lined with a piece of paper on which footprint pattern was recorded. Gait was assessed based on the following criteria: (1) hindpaw axis, defined as the angle between the direction of travel and the direction the hindpaws faced; (2) forepaw/hindpaw overlap, the distance between forepaw and hindpaw print; and (3) hindpaw width, the distance between right and left hindpaws. Mice were given a maximum of five attempts to complete the task. Failure to complete the task was operationally defined as the inability of a mouse to produce at least two consecutive sets of footprints. Mice that could not complete the task were excluded from analysis (nine *fBZ/fBZ* mice and four *Wnt1Cre;fBZ/fBZ* mice). Data were analysed using one-way ANOVA and they are expressed as mean ± S.E.M.

Motor coordination and balance were assessed at P14, P20–21 and P34 using an accelerating rotarod apparatus (AccuScan Instruments, Inc., Columbus, OH, USA). A different subset of mice was tested at each age since each mouse was killed following behavioural testing and their brains were processed accordingly for immuno-histochemical, biochemical, and/or electrophysiological experiments. Acceleration was linear from 0 to 30 r.p.m. over 240 s. Latency-to-fall was recorded over a maximum time frame of 240 s. Each subject completed nine trials, completed in sets of three trials at 15 min intervals. Data were analysed using repeated measures ANOVA and they are expressed as means ± S.E.M. Limb strength was assessed at P20–21 by the wire-hang test. Mice were placed on a wire screen, which was then inverted over a container with a padded bottom. Latency-to-fall was recorded with each subject completing three trials at 15 min intervals. Trials with latency-to-fall of less than 10 s were discarded; the maximum latency recorded was 60 s. Performance was averaged across the three trials, analysed using one-way ANOVA, and data are expressed as means ± S.E.M.

Acute cerebellar slice preparation

Wild-type, *fBZ/fBZ*, and *Wnt1Cre;fBZ/fBZ* mice were asphyxiated by CO_2 and decapitated. The cerebellum was then isolated and immersed in ice-cold artificial cerebral spinal fluid (aCSF) containing (mM) 125 NaCl, 2.5 KCl, 1 $MgCl_2.6H_2O$, 1.25 NaH_2PO_4, 2 $CaCl_2.2H_2O$, 25 $NaHCO_3$, and 25 glucose. The cerebellum was then embedded in 4% low-melting-point agar, and 200 μm parasagittal slices were cut using a vibroslicer (Electron Microscopy Sciences, Hatfield, PA, USA). All solutions used to prepare and store slices were bubbled continuously with 5% CO_2–95% O_2. For animals older than P5, the agar-embedded cerebellum was sliced in a slicing solution containing (mM) 3 KCl, 7 $MgCl_2.6H_2O$, 1.25 NaH_2PO_4, 0.5 $CaCl_2.2H_2O$, 28 $NaHCO_3$, 0.6 ascorbate, 0.1 kynurenate, 110 sucrose, and 5 glucose. The slices were then incubated in aCSF at room temperature for at least 1 h prior to electrophysiological recording.

Whole-cell patch-clamp recording, data acquisition and analysis

Slices of the cerebellar vermis were transferred to a recording chamber, maintained at 32°C on a heated stage fit onto an upright microscope (BX50WI; Olympus), and continuously perfused at rate of 0.5 ml min^{-1} with oxygenated aCSF. Cerebellar neurons were visualized under Hoffman Modulation Optics (Hoffman Modulation Optics, Greenvale, NY, USA) using a ×40 water-immersion objective (Olympus; 3 mm working distance). An analog video camera attached to a video frame grabber board (Integral Technologies, Indianapolis, IN, USA) displayed real-time images on a computer monitor, and this aided the navigation and placement of the recording and stimulating electrodes. Patch electrodes were pulled from borosilicate capillary glass (1.5 mm o.d.; Warner Instrument Corporation, Holliston, MA, USA). Once filled with recording solution, electrodes had resistances of 4–6 MΩ. The recording solution contained (mM) 60 CsCl, 10 caesium D-gluconate, 20 TEA-Cl, 4 $MgCl_2$, 30 Hepes, 2 Mg-ATP, and 3 Na-GTP. Immediately prior to each recording session, 0.15% Lucifer yellow was added to the recording solution to mark the recorded Purkinje cell. In some experiments, the recording solution also contained the lidocaine derivative QX314 (10 μM) to suppress activation of voltage-gated Na^+ channels. In addition, bicuculline

methiodide (10 μM) was included in the aCSF to minimize inhibitory synaptic activity. Recordings were made with an EPC9 amplifier (HEKA Instruments, Inc., Southboro, MA, USA). Membrane currents were filtered at 10 kHz, digitized using Pulse, and analysed off-line using PulseFit (HEKA Instruments, Inc.).

Purkinje cells in the bank and gyrus regions of the cerebellar cortex were selected for recording (Nishiyama & Linden, 2004). Purkinje cell current responses to climbing fibre activation were monitored at a holding potential of −20 mV under whole-cell patch-clamp conditions. Climbing fibre responses were evoked by passing current (0.1–10 mA) through a bipolar stimulating electrode insulated in an aCSF-containing glass pipette (3–5 μm diameter) placed in the internal granule cell layer approximately 40–80 μm away from the cell under study. Both stimulation intensity and the position of the stimulating electrode were adjusted to optimize the detection of stimulus-evoked responses. Paired-pulse ratio was obtained by two stimuli separated by an interval of 40 ms. Climbing fibre-evoked responses were identified on-line as all-or-none current responses to incremental variations in stimulus intensity (e.g. lower right insets in Fig. 3*Aa–c*) as well as by the detection of paired pulse depression (e.g. upper left insets in Fig. 3*Aa–c*). These features are unique to climbing fibre activation, *vis-à-vis* parallel fibre-evoked responses that are typically graded and exhibit paired pulse facilitation (Puro & Woodward, 1977; Silver *et al.* 1998; Kakizawa *et al.* 2000; Hashimoto & Kano, 2003; Foster & Regehr, 2004; Nishiyama & Linden, 2004). The minimum number of climbing fibres innervating a Purkinje cell was thus derived based on the number of all-or-none discrete steps that were revealed when stimulus intensity was plotted as a function of response amplitude. Figure 3*Aa–c* illustrates representative recordings from Purkinje cells at P20–24 innervated by a single climbing fibre in the wild-type (Fig. 3*Aa*) but by two climbing fibres in the *fBZ/fBZ* (Fig. 3*Ab*) and *Wnt1Cre;fBZ/fBZ* mice (Fig. 3*Ac*).

A subset of experiments assessed whether there was a correlation between latency-to-fall and the prevalence of multiply innervated Purkinje cells. To this end, climbing fibre responses were monitored in mice that had been tested using the rotarod assay. The latency-to-fall and percentage of multiple innervation measured in individual mice were compared using a linear regression.

Responses of Purkinje cells to parallel fibre activation were elicited by placing a stimulating electrode in the molecular layer of a cerebellar slice, approximately 40–80 μm away from the cell under study. Both stimulation duration and the position of the stimulating electrode were adjusted to optimize the detection of stimulus-evoked responses. While the stimulus intensities used to elicit the maximum amplitude varied between Purkinje cells, they did not vary across genotypes ($P = 0.189$ by one-way ANOVA). Paired-pulse ratio was obtained by two stimuli separated by an interval of 40 ms. Parallel fibre responses were differentiated from climbing fibre responses based upon the criteria listed above.

Rapid Golgi impregnation

Cerebella were removed and immersed in Golgi-Cox solution for 2 days (1.04% potassium dichromate, 1.04% mercuric chloride, and 0.83% potassium chromate, pH 7.0), immersed in fresh Golgi-Cox solution for 2 weeks, then in 30% sucrose in PBS for 5 days. Parasagittal sections (200 μm) of agar-embedded cerebella (4%) were cut using a vibroslicer (World Precision Instruments). Slices were then incubated for 30 min in 15% ammonia, washed with phosphate buffer (PB) containing 0.228% sodium phosphate and 0.262% sodium diphosphate, incubated in 1% thiosulphate for 30 min, and mounted and coverslipped after a final wash in PB.

Results

This study employed three groups of mice: (1) wild-type control mice; (2) *fBZ/fBZ* mice, a hypomorphic mouse line harbouring floxed TrkB alleles (Xu *et al.* 2000); and (3) *Wnt1Cre;fBZ/fBZ* mice, generated by crossing the *fBZ/fBZ* mice with the *Wnt1Cre* mouse line, thereby achieving a conditional knockout of TrkB in the hindbrain, including the cerebellum (Rico *et al.* 2002). Mice from each line were evaluated for ataxia using the footprint assay and rotarod test. Cerebellar slices were used to assess electrophysiologically climbing fibre innervation of Purkinje cells at three developmental time points: P3–5, when innervation of individual Purkinje cells by multiple climbing fibres prevails; P12–14, when regression of the multiple climbing fibre inputs is at its height; and P20–24, when the mature one-to-one pattern of CF–PC innervation is established.

TrkB hypomorphism in the cerebellar cortex of *fBZ/fBZ* and *Wnt1Cre;fBZ/fBZ* mice

Parasagittal 20 μm cerebellar cryosections obtained from wild-type, *fBZ/fBZ* and *Wnt1Cre;fBZ/fBZ* mice were processed for immunostaining with an antibody against TrkB. In P5, P14 and P21 wild-type cerebellar cortex, punctate TrkB immunoreactive profiles were broadly distributed (Fig. 1*Aa–c*). At P5, TrkB immunoreactivity was localized to calbindin-immunopositive Purkinje cells, the external granule cell layer, and differentiated granule cells in the internal granule cell layer (Fig. 1*Aa*). At P14 (Fig. 1*Ab*), TrkB immunoreactivity was localized to the molecular layer, Purkinje cell layer, and internal granule

cell layer. This pattern of TrkB immunostaining remained largely unaltered at P21 (Fig. 1*Ac* and *Ba*).

In the cerebellar cortex of *fBZ/fBZ* mice, the most consistent deviation in TrkB immunostaining compared to wild-type mice was a qualitative decrease in fluorescence intensity. This decrease was uniform, insofar as it was not specific to any of the cerebellar cortical layers (Fig. 1*Bb*). As expected, and in striking contrast to that seen in the wild-type and *fBZ/fBZ* mice, virtually no TrkB immunoreactivity was detected in the cerebellar cortex of the *Wnt1Cre;fBZ/fBZ* mice (Fig. 1*Bc*).

Western blot analysis of cerebella from the three groups of mice confirmed our immunohistochemical observations (Fig. 1*C–E*). Figure 1*D* illustrates that, when normalized to whole brain protein extract, P14 *fBZ/fBZ* mice expressed 38% ($n = 21$ cerebella) and *Wnt1Cre;fBZ/fBZ* mice expressed 7% ($n = 12$ cerebella) of the TrkB protein as their age-matched wild-type counterparts ($n = 24$ cerebella). TrkB protein levels were significantly diminished in both lines of mutant mice *vis-à-vis* wild-type mice ($P < 0.001$). Similar results were obtained at P20, when *fBZ/fBZ* mice expressed 18% ($n = 21$ cerebella) and *Wnt1Cre;fBZ/fBZ* mice expressed 7% ($n = 29$ cerebella) of the TrkB protein assayed in wild-type mice ($n = 75$ cerebella; $P < 0.001$; Fig. 1*E*). These findings are in overall agreement with earlier studies reporting decreased levels of TrkB expression in the *fBZ/fBZ* and *Wnt1Cre;fBZ/fBZ* mouse lines (Xu *et al.* 2000; Rico *et al.* 2002).

ELISAs were also performed on cerebella from wild-type, *fBZ/fBZ*, and *Wnt1Cre;fBZ/fBZ* mice. The ratio of BDNF to total protein was 0.0171 ± 0.0065 in wild-type mice ($n = 63$ cerebella), 0.0829 ± 0.0581 in *fBZ/fBZ* mice ($n = 26$ cerebella), and 0.0406 ± 0.0280 in *Wnt1Cre;fBZ/fBZ* mice ($n = 5$ cerebella). While there appeared to be a trend for BDNF levels to be higher in the TrkB mutants, particularly in the *fBZ/fBZ* mice, this was not statistically different from those assessed in wild-type mice ($P = 0.222$).

Motor coordination and balance in TrkB hypomorphic and null mice

Mice harbouring a knockout of BDNF are ataxic (Schwartz *et al.* 1997). In the present study, the *fBZ/fBZ* and *Wnt1Cre;fBZ/fBZ* mice exhibited abnormal gait and, if suspended by the tail, displayed a clasping/crossing phenotype typical of motor and balance abnormalities which have been associated with dysfunction in brain regions involved in motor control, including the cerebellum (Lalonde, 1987*a*,*b*; Baquet *et al.* 2005). A footprint assay, as depicted in Fig. 2*A*, revealed that the

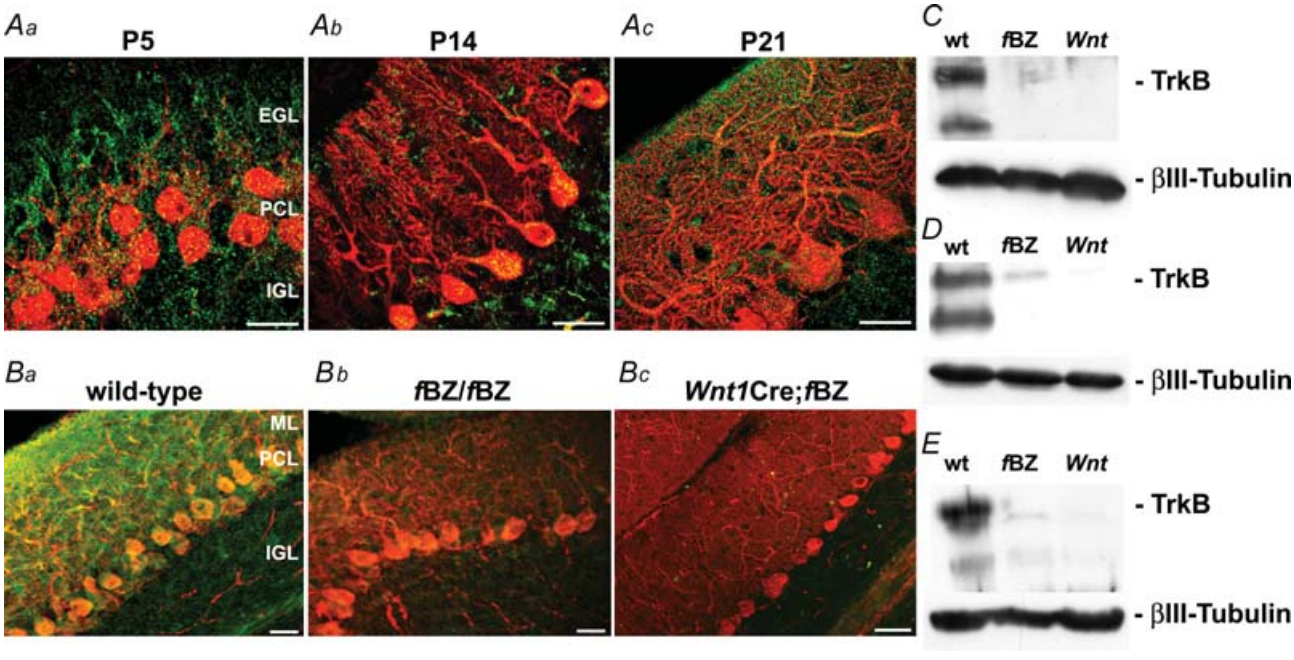

Figure 1. TrkB expression during cerebellar development under normal, TrkB-hypomorphic and TrkB-null conditions
A, calbindin (red) and TrkB (green) immunostaining in the cerebellar cortex at postnatal day (P)5 (*a*), P14 (*b*), and P21 (c) in wild-type mice. Scale bars (*Aa* and *b*), 10 μm; (*Ac*), 20 μm. *B*, calbindin (red) and TrkB (green) immunostaining of wild-type (*a*), *fBZ/fBZ* (*b*), and *Wnt1Cre;fBZ/fBZ* (c) cerebella. Scale bars, 20 μm. *C–E*, Western blots of homogenized cerebella from wild-type (wt), *fBZ/fBZ* (*fBZ*), and *Wnt1Cre;fBZ/fBZ* (*Wnt*) mice at P4 (*C*), P14 (*D*), and P21 (*E*). TrkB expression was normalized to βIII-tubulin.

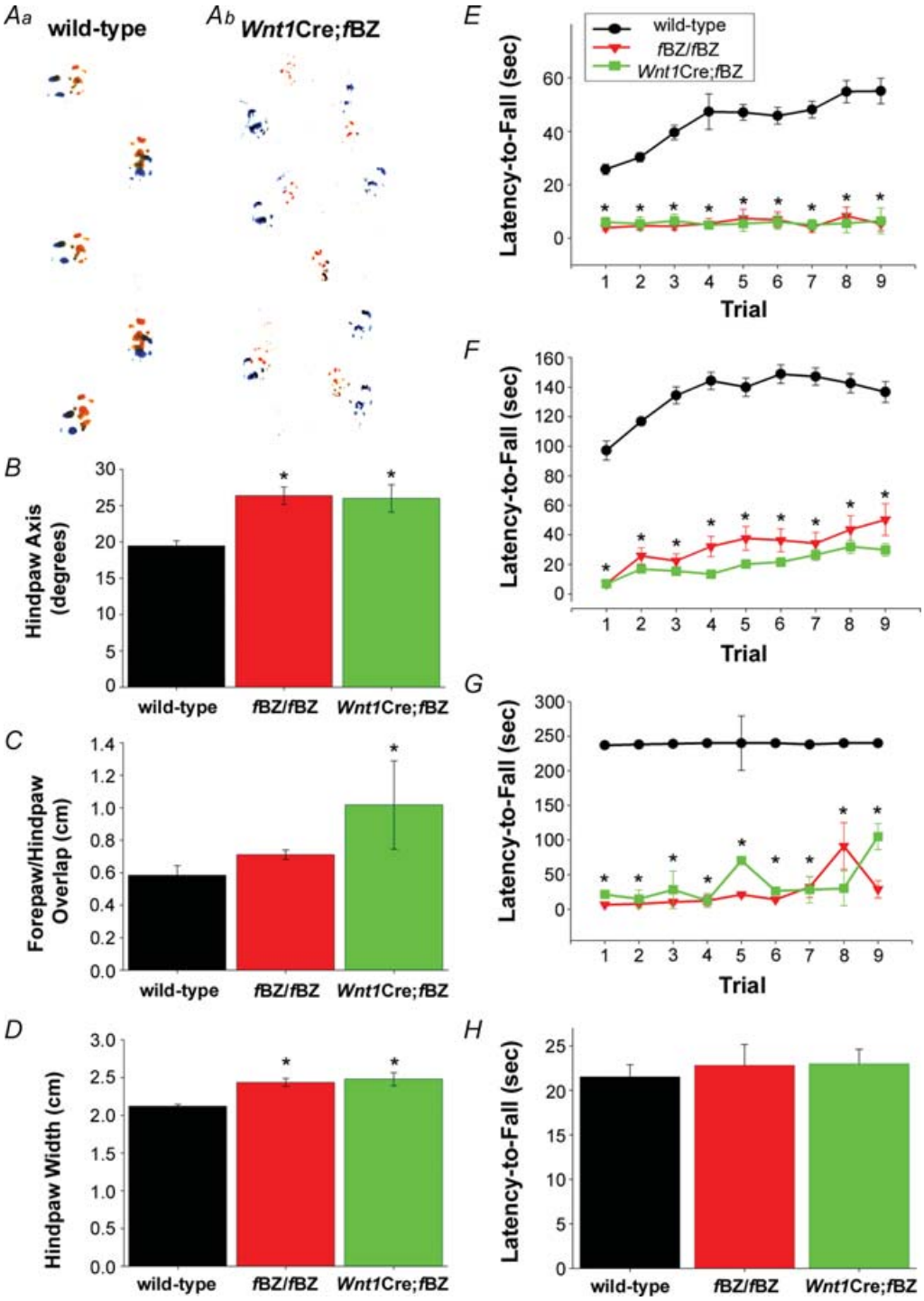

Figure 2. TrkB mutant mice are ataxic
A, representative footprint traces from a wild-type (*a*) and a *Wnt1Cre;fBZ/fBZ* (*b*) mouse at P20. *B–D*, footprint traces were analysed based upon the hindpaw axis (*B*), the forepaw/hindpaw overlap (*C*), and hindpaw width (*D*). At P20–24, *fBZ/fBZ* mice had significantly wider hindpaw axes and width than wild-type mice; *Wnt1Cre;fBZ/fBZ* mice had wider hindpaw axes, greater distance between the fore and hindpaw prints, and wider hindpaw width than wild-type mice (*$P < 0.001$ by one-way ANOVA). *E–G*, rotarod performance in wild-type (black circles), *fBZ/fBZ* (red triangles), and *Wnt1Cre;fBZ/fBZ* (green squares) mice at P14 (*E*), P20 (*F*), and P34 (*G*). Each symbol represents performance assessed by averaging latency-to-fall (s) across nine trials of testing. Wild-type mice performed significantly better than *fBZ/fBZ* and *Wnt1Cre;fBZ/fBZ* mice at P14, P20 and P34 (*$P < 0.001$ by repeated-measures ANOVA). *H*, performance on the wire-hang task by wild-type, *fBZ/fBZ* and *Wnt1Cre;fBZ/fBZ* mice at P20. Latency-to-fall (s) did not differ between the three groups of mice ($P = 0.763$ by one-way ANOVA).

gait of *Wnt1Cre*;*fBZ*/*fBZ* mice was irregular compared with that of wild-type mice. Footprint data were difficult to obtain, as approximately 20% of the *fBZ*/*fBZ* and *Wnt1Cre*;*fBZ*/*fBZ* mice could not complete the task, either falling over or circling instead of walking in a straight line. This tended to skew our footprint data towards a more normal gait. An ataxic gait was defined by a shorter, wider gait, with the hindpaws splayed outward and little overlap between the forepaw and hindpaw (Carter *et al.* 1999). The hindpaws of *fBZ*/*fBZ* ($n = 33$) mice were splayed outward at an angle of 26.4 ± 1.9 deg, and at an angle of 26.0 ± 1.9 deg in the *Wnt1Cre*;*fBZ*/*fBZ* ($n = 14$) mice; these measurements were significantly wider than for wild-type mice (19.4 ± 0.71 deg; $n = 60$; $P < 0.001$; Fig. 2*B*). The footprints of *Wnt1Cre*;*fBZ*/*fBZ* mice (1.02 ± 0.27 cm; $n = 14$) overlapped significantly less than wild-type mice (0.58 ± 0.06 cm; $n = 60$; $P = 0.017$; Fig. 2*C*). The gait of the *fBZ*/*fBZ* and *Wnt1Cre*;*fBZ*/*fBZ* mice was significantly wider than their wild-type counterparts, as revealed by hindpaw width ($P < 0.001$; Fig. 2*D*). The average hindpaw width was 2.12 ± 0.03 cm in wild-type ($n = 60$), 2.43 ± 0.05 cm in *fBZ*/*fBZ* ($n = 33$), and 2.48 ± 0.09 cm in *Wnt1Cre*;*fBZ*/*fBZ* mice ($n = 14$). Thus, TrkB mutant mice characteristically displayed an ataxic gait.

We also employed the rotarod test to assess motor coordination and balance at P14, P20 and P34. Behavioural testing was not conducted in the P3–5 age group since motor coordination has not yet developed and eye-opening has not yet occurred. Performance was evaluated based on the length of time the subject remained on a rod rotated at a linearly accelerating speed (0–30 r.p.m., maximum time 240 s; Jones & Roberts, 1968; Crawley, 1999).

At P14, latency-to-fall was 37.9 ± 2.8 s for wild-type ($n = 57$), 7.5 ± 3.1 s for *fBZ*/*fBZ* ($n = 42$), and 6.9 ± 3.2 s for *Wnt1Cre*;*fBZ*/*fBZ* mice ($n = 17$). P14 wild-type mice performed significantly better than either *fBZ*/*fBZ*

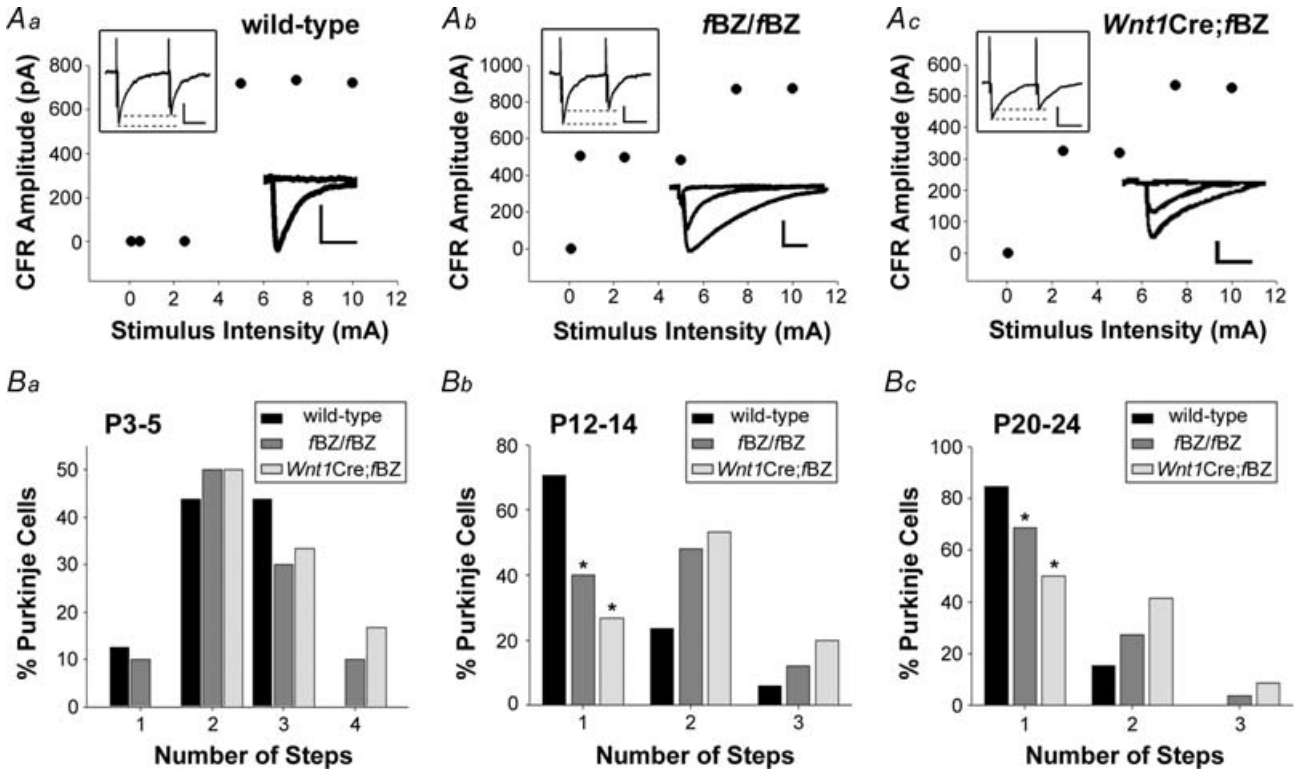

Figure 3. Purkinje cells remain innervated by multiple climbing fibres in TrkB mutant mice
A, plots of climbing fibre response (CFR) amplitude *versus* stimulus intensity from Purkinje cells of P20–24 wild-type (*a*), *fBZ*/*fBZ* (*b*), and *Wnt1Cre*;*fBZ*/*fBZ* (*c*) cerebella. The lower right insets are representative of the CFRs used to generate the plots. Scale bars: vertical, 200 pA; horizontal, 10 ms. The upper left insets depict paired pulse depression upon climbing fibre activation. Scale bars: vertical, 250 pA; horizontal, 10 ms. *B*, the percentage of Purkinje cells recorded with 1, 2, 3 or 4 CFRs (steps) at P3–5 (*a*), P12–14 (*b*), and P20–24 (*c*). (P3–5: $n = 15$ wild-type cells, $n = 11$ *fBZ*/*fBZ* cells, and $n = 6$ *Wnt1Cre*;*fBZ*/*fBZ* cells; P12–14: $n = 19$ wild-type cells, $n = 26$ *fBZ*/*fBZ* cells, and $n = 15$ *Wnt1Cre*;*fBZ*/*fBZ* cells; P20–24: $n = 71$ wild-type cells, $n = 68$ *fBZ*/*fBZ* cells, and $n = 52$ *Wnt1Cre*;*fBZ*/*fBZ* cells). At P12–14 (*Bb*) and P20–24 (*Bc*), a larger percentage of Purkinje cells retain multiple innervation in the TrkB mutant (*fBZ*/*fBZ* and *Wnt1Cre*;*fBZ*/*fBZ*) mice as compared with the wild-type mice (P12–14: $\chi^2 = 15.9$, $^*P < 0.001$; P20–24: $\chi^2 = 18.9$, $^*P < 0.001$ by χ^2 test).

or *Wnt1Cre;fBZ/fBZ* mice ($P < 0.001$; Fig. 2*E*). By P20, performance on the rotarod by *fBZ/fBZ* and *Wnt1Cre;fBZ/fBZ* mice was further exacerbated ($P < 0.001$; Fig. 2*F*); latency-to-fall was 148.9 ± 6.5 s for wild-type ($n = 142$), 24.2 ± 9.7 s for *fBZ/fBZ* ($n = 36$), and 16.1 ± 3.1 s for *Wnt1Cre;fBZ/fBZ* mice ($n = 52$). Poor performance on the rotarod task was still evident in both the *fBZ/fBZ* and *Wnt1Cre;fBZ/fBZ* mice at P34, when the wild-type mice displayed a significantly longer latency-to-fall (234.9 ± 4.4 s, $n = 5$) than either the *fBZ/fBZ* (25.2 ± 5.0 s, $n = 7$) or the *Wnt1Cre;fBZ/fBZ* mice (37.6 ± 5.2 s, $n = 2$; $P < 0.001$; Fig. 2*G*).

At P20, the mutant mice were significantly smaller than their wild-type littermates (wild-type: 8.74 ± 0.194 g, $n = 109$; *fBZ/fBZ*: 7.80 ± 0.335 g, $n = 27$; *Wnt1Cre;fBZ/fBZ*: 8.09 ± 0.286 g, $n = 50$; $P = 0.034$), and this could affect limb strength. However, further analysis revealed that limb weakness did not contribute to the poor performance of the *fBZ/fBZ* and *Wnt1Cre;fBZ/fBZ* mice on the rotarod. First, cross analysis of the rotarod and body mass data sets revealed no correlation between performance on the rotarod and body mass in wild-type ($r^2 = 0.01$, $n = 110$), *fBZ/fBZ* ($r^2 = 0.37$, $n = 28$), or *Wnt1Cre;fBZ/fBZ* ($r^2 = 0.04$, $n = 49$) mice. Second, performance was compared across ages based on the premise that younger, smaller mice may be weaker. *fBZ/fBZ* and *Wnt1Cre;fBZ/fBZ* mice exhibited significantly shorter latency-to-fall than younger wild-type mice of similar size ($P < 0.001$). Third, limb strength was assessed using the wire-hang test in a subgroup of P20 mice that had completed the rotarod task. Wild-type (21.5 ± 1.4 s, $n = 34$), *fBZ/fBZ* (22.8 ± 2.3 s, $n = 11$), and *Wnt1Cre;fBZ/fBZ* (23.0 ± 1.6 s, $n = 21$) mice performed similarly on this task ($P = 0.763$; Fig. 2*H*). Thus, TrkB mutant mice were not motorically weaker. The results of the behavioural experiments, taken together, indicated that ataxia, rather than size or limb strength, accounted for the poor rotarod performance of the *fBZ/fBZ* and *Wnt1Cre;fBZ/fBZ* mice.

Climbing fibre innervation of Purkinje cells in TrkB mutant mice

In rodents, experimental or genetic manipulations that disrupt pruning at the CF–PC synapse during cerebellar development are often associated with abnormalities in motor coordination and balance (Offermanns *et al.* 1997; Kano *et al.* 1998; Ichise *et al.* 2000; Ribar *et al.* 2000). Climbing fibre innervation was assessed by monitoring climbing fibre-evoked whole-cell current responses of Purkinje cells in 200 μm parasagittal cerebellar slices derived from wild-type, *fBZ/fBZ*, and *Wnt1Cre;fBZ/fBZ* mice.

At P3–5, prior to the onset of synaptic pruning, a comparable number of all-or-none climbing fibre responses (i.e. steps) was detected across genotypes. The percentage of Purkinje cells displaying single or multiple climbing fibre innervation was also comparable between the three groups of mice ($\chi^2 = 3.4$, $P = 0.756$; Fig. 3*Ba*). By P12–14, a significant shift toward mono-innervation was evident in wild-type cerebellum ($\chi^2 = 12.4$, $P = 0.002$; Fig. 3*Bb*). In *fBZ/fBZ* and *Wnt1Cre;fBZ/fBZ* mice, this shift was statistically insignificant compared with their P3–5 counterparts (*fBZ/fBZ*: $\chi^2 = 5.9$, $P = 0.117$; *Wnt1Cre;fBZ/fBZ*: $\chi^2 = 5.9$, $P = 0.117$). Furthermore, at P12–14, *fBZ/fBZ* and *Wnt1Cre;fBZ/fBZ* mice had significantly more multiply innervated Purkinje cells than wild-type mice ($\chi^2 = 15.9$, $P < 0.001$; Fig. 3*Bb*). By P20–24, synapse elimination had occurred in all three groups of mice as the incidence of encountering mono-innervated cerebellar Purkinje cells increased compared with their P3–5 counterparts (wild-type: $\chi^2 = 46.9$, $P < 0.001$; *fBZ/fBZ*: $\chi^2 = 23.4$, $P < 0.001$; *Wnt1Cre;fBZ/fBZ*: $\chi^2 = 17.8$, $P = 0.007$; Fig. 3*Bc*). However, a significantly higher percentage of Purkinje cells remained multiply innervated by climbing fibres in the TrkB mutant mice compared with the wild-type mice ($\chi^2 = 18.9$, $P < 0.001$; Fig. 3*Bc*). These results indicated that (1) TrkB did not influence the initial investment of climbing fibres at the forming the CF–PC synapse and (2) conditions that perturbed cerebellar TrkB expression were often associated with atypical pruning of climbing fibre contacts.

To investigate a potential link between ataxia and the persistence of Purkinje cells innervated by multiple climbing fibres, we obtained electrophysiological data from behaviourally tested mice. Mice were first evaluated for performance on the rotarod at P20 (Fig. 4*A*). In agreement with the results of the general survey on ataxia (Fig. 2*B–D* and *F*), the TrkB mutant mice displayed impaired motor coordination, as latency-to-fall was significantly longer in wild-type ($n = 9$) than *fBZ/fBZ* ($n = 6$) and *Wnt1Cre;fBZ/fBZ* ($n = 11$) mice ($P < 0.001$; Fig. 4*A*). Parasagittal cerebellar slices were then obtained from each mouse at P21–24 to assess electrophysiologically the disposition of climbing fibre innervation (Fig. 4*B*). In the wild-type mice, 82% of the Purkinje cells examined were mono-innervated, and the remaining 18% were innervated by two climbing fibres. In the *fBZ/fBZ* and *Wnt1Cre;fBZ/fBZ* mice, a higher percentage of Purkinje cells were dually innervated (27 and 32%, respectively). Notably, Purkinje cells innervated by three or more climbing fibres were never encountered in wild-type cerebella, but could be demonstrated in cerebellar slices from *fBZ/fBZ* and *Wnt1Cre;fBZ/fBZ* mice. Comparing behavioural and electrophysiological data from individual mice, there was a significant correlation between poor motor coordination and the

prevalence of multiple climbing fibre innervation ($r^2 = 0.448$; $P = 0.034$).

We then asked whether the intrinsic properties of the evoked climbing fibre response are altered in the *fBZ/fBZ* and *Wnt1Cre;fBZ/fBZ* mice, since this could be one mechanism by which multiple climbing fibre innervation persists. Paired-pulse ratio was assessed in individual Purkinje cells from P20–24 mice and analysed in terms of genotype and the number of innervating climbing fibres was similar between the wild-type and TrkB mutant mice (Fig. 4*C*). The climbing fibre response with the largest amplitude was selected for analysis multiply innervated Purkinje cells. In wild-type mice, the paired-pulse ratio was 0.82 ± 0.018 in mono-innervated Purkinje cells and 0.83 ± 0.028 in dually innervated Purkinje cells ($n = 54$ total cells). In *fBZ/fBZ* mice, the paired-pulse ratio was 0.83 ± 0.015 in mono-innervated Purkinje cells, 0.81 ± 0.047 in dually innervated Purkinje cells, and 0.76 ± 0.140 in triply innervated Purkinje cells ($n = 47$ total cells). In *Wnt1Cre;fBZ/fBZ* mice, the paired-pulse ratio was 0.82 ± 0.034 in mono-innervated Purkinje cells, 0.76 ± 0.140 in dually innervated Purkinje cells, and 0.81 ± 0.012 in triply innervated Purkinje cells ($n = 40$ total cells). Thus, at the developing CF–PC synapse, TrkB did not influence paired-pulse ratio, which is an indicator of release probability at presynaptic sites (Stevens & Wang, 1995; Silver *et al.* 1998).

Our analysis also revealed no difference in the amplitude of the evoked climbing fibre responses across genotypes. The amplitude of the largest evoked climbing fibre response was 715.6 ± 68.1 pA in wild-type mice, 904.1 ± 94.5 pA in *fBZ/fBZ* mice, and 656.7 ± 68.3 pA in *Wnt1Cre;fBZ/fBZ* mice. The largest evoked climbing fibre response did not vary across genotype ($P = 0.082$;

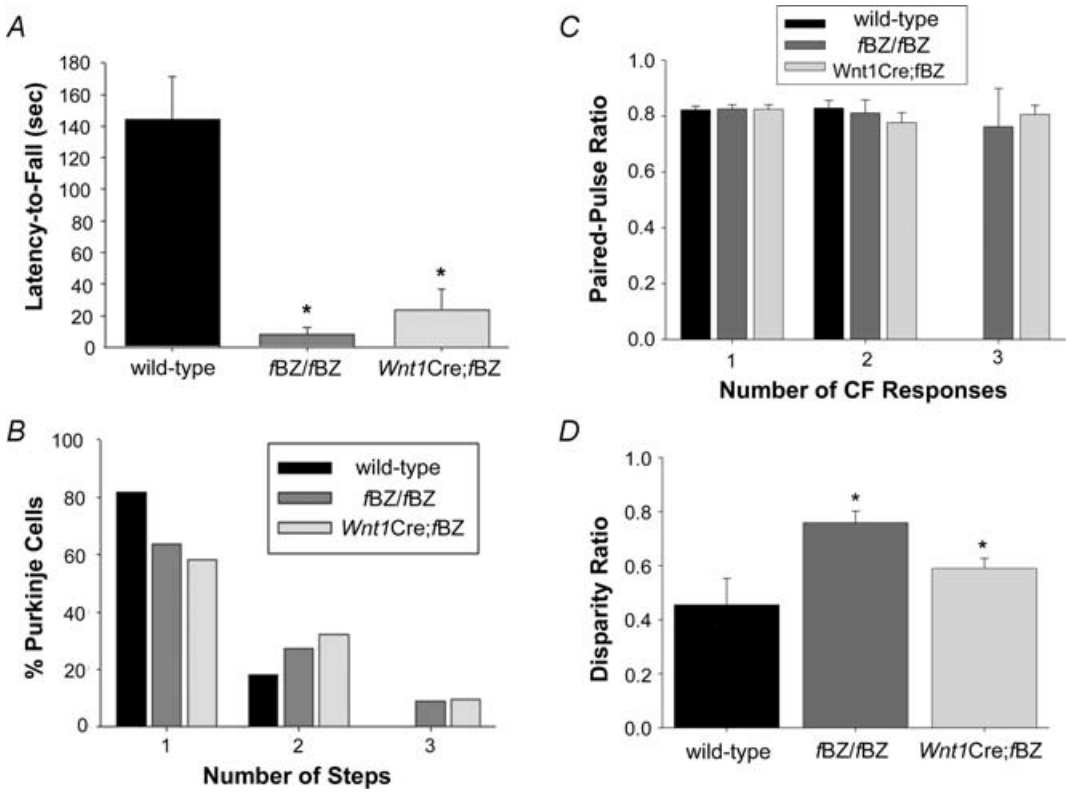

Figure 4. Persistence of Purkinje cell innervation by multiple climbing fibres is associated with ataxia and increased disparity ratio

A, rotarod performance at P20 of wild-type, *fBZ/fBZ* and *Wnt1Cre;fBZ/fBZ* mice. Data represent the subset of rotarod-tested mice that were subsequently used in electrophysiological studies. The wild-type mice performed significantly better than the *fBZ/fBZ* and *Wnt1Cre;fBZ/fBZ* mice (*$P < 0.001$ by repeated measures ANOVA). *B*, the percentage of Purkinje cells recorded with 1, 2 or 3 CFRs (steps) at P21–24 from the behaviourally tested mice illustrated in *A* ($n = 22$ wild-type cells, $n = 11$ *fBZ/fBZ* cells, and $n = 31$ *Wnt1Cre;fBZ/fBZ* cells). *C*, paired-pulse ratio at P20–24 of wild-type, *fBZ/fBZ* and *Wnt1Cre;fBZ/fBZ* mice, based on whether 1, 2 or 3 CF responses were evoked in a given Purkinje cell. Paired-pulse ratio did not vary significantly with either genotype or the degree of multiple innervation ($P = 0.492$, 0.866 by two-way ANOVA). *D*, disparity ratio of CF responses in multiply innervated Purkinje cells was significantly greater in TrkB mutant mice than in wild-type at P20–24 (*$P = 0.037$ by one-way ANOVA). Disparity ratio was defined as the average of the ratios between the smaller amplitude responses to that with the greatest amplitude.

one-way ANOVA). In Purkinje cells innervated by more than one climbing fibre, the amplitude of the weaker response(s) also did not vary across genotype ($P = 0.079$; one-way ANOVA). The amplitude of the second largest evoked climbing fibre response was 289.3 ± 118.1 pA in wild-type mice, 857.3 ± 194.3 pA in *fBZ/fBZ* mice, and 504.4 ± 80.4 pA in *Wnt1Cre;fBZ/fBZ* mice.

Competition between multiple climbing fibres innervating an individual Purkinje cell has been implicated in the process of synaptic pruning at the CF–PC synapse. In this scenario, an immature multiply innervated Purkinje cell is classified as being innervated by strong and weak climbing fibres based on the amplitude of stimulus-evoked responses. As development progresses, the stronger fibre increases in amplitude, and stabilizes, while the weaker ones regress. We compared the amplitude of climbing fibre responses in multiply innervated Purkinje cells recorded in wild-type, *fBZ/fBZ*, and *Wnt1Cre;fBZ/fBZ* mice using a disparity ratio (Hashimoto & Kano, 2003). The disparity ratio was 0.46 ± 0.098 in wild-type mice ($n = 6$ cells), 0.74 ± 0.037 in *fBZ/fBZ* mice ($n = 8$ cells), and 0.59 ± 0.036 in *Wnt1Cre;fBZ/fBZ* mice ($n = 21$ cells). Thus, the disparity ratios of both TrkB mutant mice were significantly greater than wild-type mice ($P = 0.037$; Fig. 4*D*), suggesting that depletion or deletion of TrkB impaired competition between the various climbing fibres innervating an individual Purkinje cell.

Translocation of climbing fibre contacts *vis-à-vis* synaptic pruning in developing Purkinje cells

The dynamics of synaptic reorganization at the developing CF–PC synapse extend beyond the pruning of supernumerary climbing fibre contacts to include a concomitant translocation of these contacts from the soma to the dendrites as immature Purkinje cells elaborate their dendritic arbour (Mason *et al.* 1990; Bravin *et al.* 1995; Overbeck & King, 1999; Morara *et al.* 2001; Scelfo *et al.* 2003; Sugihara, 2005). Indeed, perturbation of the pruning of supernumerary contacts in the course of CF–PC synaptic development is often associated with abnormal climbing fibre synaptic profiles (Hashimoto *et al.* 2001; Ichikawa *et al.* 2002; Miyazaki *et al.* 2004; Cesa & Strata, 2005; Hirai *et al.* 2005). In this light, we assessed whether synaptic pruning depends on translocation as climbing fibre contacts reorganize at the developing CF–PC synapse. The vesicular glutamate transporters (VGluT) 1 and 2 have been reported to be effective markers of parallel and climbing fibre terminals, respectively (Fremeau *et al.* 2001, 2004; Hisano *et al.* 2002; Kaneko & Fujiyama, 2002; Miyazaki *et al.* 2003). In Fig. 5*A*, VGluT1 immunostaining preferentially labelled parallel fibre terminals in the molecular layer. No apparent differences were observed when VGluT1 immunoreactivity was compared across genotypes (Fig. 5*B–D*). In contrast, VGluT2 immunoreactive profiles outlined the contour of calbindin-immunopositive Purkinje cell dendrites, consistent with the topographical distribution of climbing fibre terminals (Fig. 5*A*). VGluT2 immunostaining also revealed that the innervation field of climbing fibres translocated from the Purkinje cell soma at P4 (Fig. 6*A*) to the proximal dendrite by P22 (Fig. 6*B*).

Given the impaired pruning of climbing fibre contacts in TrkB mutant mice, we postulated that translocation of VGluT2 immunoreactive puncta would be commensurately aberrant. However, when surveyed at P20, there was no obvious difference in the overall pattern of VGluT2 immunoreactive puncta between the cerebellar cortex of wild-type, *fBZ/fBZ*, and *Wnt1Cre;fBZ/fBZ* mice (Fig. 7*A–C*). In all cases, while VGluT2 immunoreactive puncta decorated the dendritic arbour of Purkinje cells, only a small percentage of the

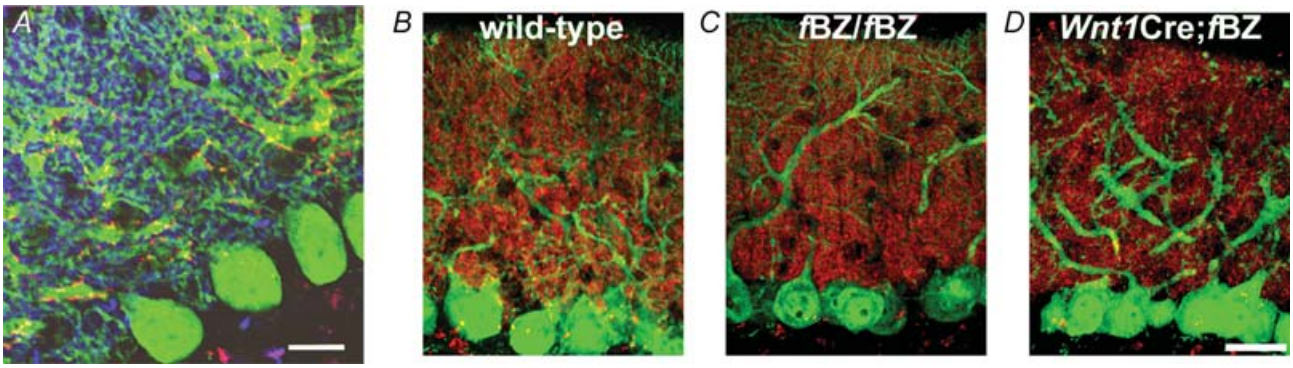

Figure 5. VGluT1 labels parallel fibre terminals in the molecular layer of the cerebellar cortex
A, differential labelling of climbing fibre and parallel fibre terminals at P21 by VGluT2 (red) and VGluT1 (blue), respectively. Purkinje cells were immunolabelled with calbindin (green). Scale bar, 20 μm. *B–D*, VGluT1 (red) and calbindin (green) immunoreactivity in wild-type (*B*), *fBZ/fBZ* (*C*), and *Wnt1Cre;fBZ/fBZ* (*D*) mice at P21. Scale bar, 20 μm.

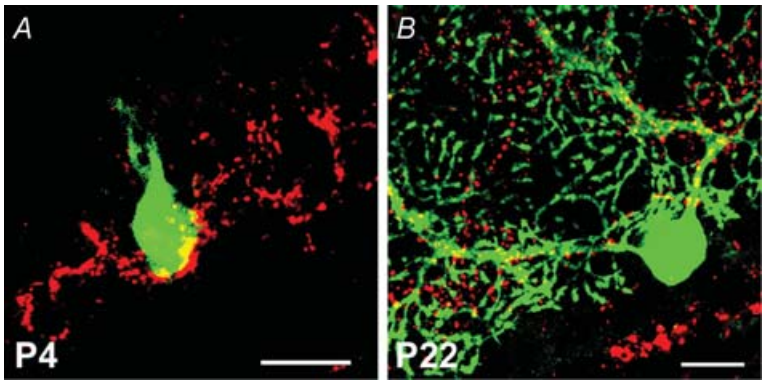

Figure 6. VGluT2 immunostaining reveals CF terminals and their translocation during cerebellar development
A, innervation field of climbing fibres on a multiply innervated, Lucifer-yellow-filled Purkinje cell (green) in a P4 wild-type cerebellar slice. Climbing fibre terminals are labelled with a VGluT2 antibody (red) and restricted to the Purkinje cell soma (colocalization: yellow). Scale bar, 20 μm. *B*, by P22, the climbing fibre innervation field has translocated to the dendrite of this mono-innervated Purkinje cell. Scale bar, 20 μm.

Purkinje cells had VGluT2 immunoreactive puncta on the soma (wild-type: 5.9%, $n = 163$ cells; *fBZ/fBZ*: 6.7%, $n = 96$ cells; *Wnt1Cre;fBZ/fBZ*: 13.7%, $n = 130$ cells). Translocation of climbing fibre contacts had occurred to an equivalent extent in the wild-type and TrkB mutant cerebella ($P = 0.727$). Furthermore, the extent of VGluT2 innervation within the molecular layer, quantified as a ratio between the furthest extent of VGluT2 immunoreactive puncta and the pial surface of the cerebellar cortex, also did not vary across genotypes ($P = 0.483$; Fig. 7*D*). This ratio was 0.652 ± 0.020 in wild-type, 0.684 ± 0.029 in *fBZ/fBZ*, and 0.635 ± 0.028 in *Wnt1Cre;fBZ/fBZ* mice.

Climbing fibre terminals on individual electrophysiologically examined Purkinje cells were analysed to optimize correlation between pruning and translocation of climbing fibre synaptic contacts. Following each recording session, slices containing Purkinje cells that had been assessed for climbing fibre innervation and filled with Lucifer yellow were fixed and processed for VGluT2 immunostaining. This facilitated a direct correlation between the distribution of VGluT2 immunoreactive puncta and the extent of climbing fibre innervation in individual Purkinje cells (Fig. 8*A* and *B*). At P3–5, the Purkinje cells recorded were uniformly innervated by multiple climbing fibres, and all displayed a similar VGluT2 immunostaining pattern, hallmarked by immunoreactive puncta covering the soma of the recorded Purkinje cells (Fig. 8*Aa–c*).

At P20–24, mono-innervation in individual Purkinje cells with climbing fibres that had translocated to the proximal dendrite was readily demonstrable in the wild-type cerebellum (Fig. 8*Ba*). However, translocation could also be demonstrated in Purkinje cells that were innervated by multiple climbing fibres in the TrkB mutant cerebellum (Fig. 8*Bc*). The Purkinje cell from an *fBZ/fBZ* cerebellum shown in Fig. 8*Bb* was mono-innervated, while the one from a *Wnt1Cre;fBZ/fBZ* cerebellum shown in Fig. 8*Bc* was dually innervated. In both cases, the climbing fibre terminals traverse along the proximal dendritic arbour. Analysis of the density of VGluT2 immunoreactive puncta along the proximal and distal dendrites of Purkinje cells recorded at P20–24 revealed no difference between the three groups of mice (proximal: $P = 0.185$; distal: $P = 0.541$; Fig. 8*C*). These results indicated that translocation occurred regardless of the disposition of climbing fibre innervation of a given Purkinje cell ($\chi^2 = 0.3$, $P = 0.615$). Thus, TrkB, while affecting the pruning of climbing fibre contacts, did not influence the translocation of the climbing fibre terminals.

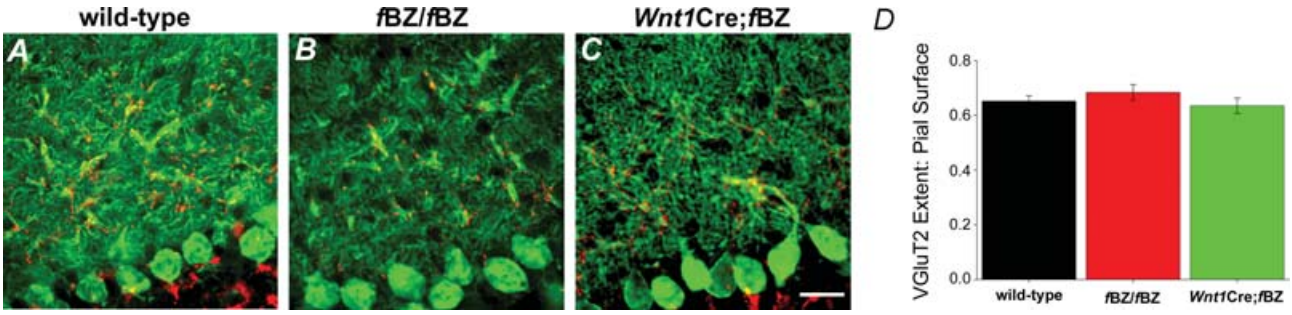

Figure 7. Climbing fibres translocate normally in the cerebellar cortex of TrkB mutant mice
A–C, VGluT2-immunopositive climbing fibre terminals (red) along the proximal dendrites of calbindin-stained Purkinje cells (green) in wild-type (*A*), *fBZ/fBZ* (*B*), and *Wnt1Cre;fBZ/fBZ* mice (*C*) at P21. Scale bar, 20 μm. *D*, extent of VGluT2 immunostaining in the molecular layer compared with the pial surface did not differ between wild-type ($n = 13$ cerebella), *fBZ/fBZ* ($n = 15$ cerebella), and *Wnt1Cre;fBZ/fBZ* ($n = 9$ cerebella) mice ($P = 0.483$ by one-way ANOVA).

Purkinje cell dendritic development and parallel fibre transmission in TrkB mutant mice. Since impaired dendritic growth could potentially influence synaptic pruning and translocation, we examined dendritic development by measuring the length of the primary dendrite and by analysing the primary, secondary and tertiary branching pattern of Golgi-impregnated Purkinje cells from wild-type and *fBZ/fBZ* mice

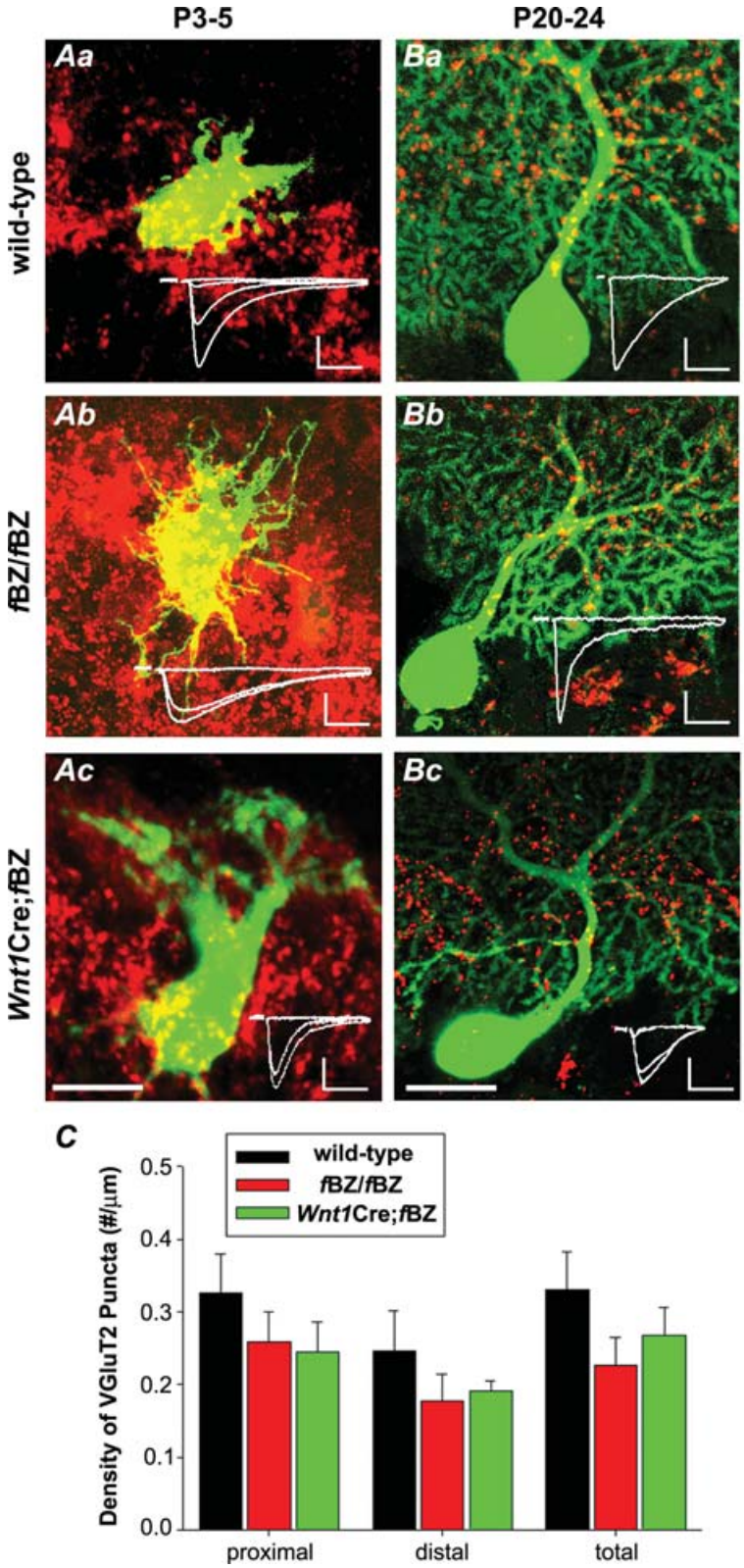

Figure 8. Translocation occurs despite absence of synapse elimination
A, VGluT2-immunoreactive climbing fibre synaptic terminals at P3–5 on three Lucifer-yellow-filled Purkinje cells, one each from a wild-type (*a*), *fBZ/fBZ* (*b*), and *Wnt1Cre*;*fBZ/fBZ* (*c*) cerebellum. Scale bar, 20 μm. The superimposed traces in the insets (*a*–*c*) indicate that all three Purkinje cells are innervated by at least two climbing fibres. Scale bars: vertical, 200 pA; horizontal, 10 ms. *B*, VGluT2-immunoreactive climbing fibre terminals at P20–24 on Lucifer-yellow-filled Purkinje cells recorded in wild-type (*a*), *fBZ/fBZ* (*b*), and *Wnt1Cre*;*fBZ/fBZ* (*c*) cerebellar slices. Scale bar, 20 μm. In the insets, the superimposed traces in *Ba* and *b* indicate that these Purkinje cells were mono-innervated, while the Purkinje cell in *Bc* was dually innervated. Regardless of whether or not the Purkinje cell was multiply innervated, VGluT2 immunoreactive puncta translocated from the soma to the dendrite. Scale bars: vertical, 200 pA; horizontal, 10 ms. *C*, quantification of the density of VGluT2 immunoreactive puncta along Purkinje cell dendrites at P20–24 from electrophysiologically recorded, Lucifer-yellow-filled Purkinje cells. Density was calculated as the number of VGluT2 immunoreactive puncta over the measured dendritic length (μm). 'Proximal' was operationally defined as the first 40 μm segment and 'distal' as the adjoining 40–120 μm segment of the Purkinje cell dendrite. There was no difference in the density of VGluT2 immunoreactive puncta between wild-type ($n = 9$ cells), *fBZ/fBZ* ($n = 8$ cells), and *Wnt1Cre*;*fBZ/fBZ* ($n = 9$ cells) mice ($P = 0.615$ by one-way ANOVA).

(Fig. 9*A–B*). At P14, Purkinje cells in *fBZ/fBZ* cerebellum exhibited significantly shorter primary dendrites and fewer secondary and tertiary dendritic branch points ($n = 185$ cells) than those in the wild-type cerebellum ($n = 175$ cells; $P < 0.001$ for both dendritic length and number of dendritic branch points; Fig. 9*C* and *D*). At P21, the primary dendrites of Purkinje cells in *fBZ/fBZ* cerebellum ($n = 26$ cells) were still shorter ($P < 0.001$) than those in the wild-type cerebellum ($n = 52$ cells), but the difference in the number of dendritic branch points seen at P14 was no longer evident ($P = 0.079$). Similar results were obtained in *Wnt1Cre;fBZ/fBZ* mice when the dendritic arbour of electrophysiologically recorded, Lucifer-yellow-filled cells were analysed (data not shown).

The similarity in dendritic branching pattern in the P20–24 age group across genotypes suggests that parallel fibre innervation within its target territory in the molecular layer may be normal at later stages of cerebellar development even when TrkB is depleted. Indeed, when parallel fibre-activated synaptic responses were examined in Purkinje cells between P20 and 24, neither the amplitude nor the paired-pulse ratio varied across genotypes ($P = 0.930$ and 0.632, respectively). The mean peak amplitude was 138.9 ± 57.5 pA in wild-type ($n = 11$ cells), 162.5 ± 56.5 pA in *fBZ/fBZ* ($n = 12$ cells), and 171.7 ± 71.5 pA in *Wnt1Cre;fBZ/fBZ* ($n = 11$ cells) mice (Fig. 9*E*). Paired-pulse ratio, analysed in the same cells, was 1.65 ± 0.088 in wild-type, 1.55 ± 0.148 in *fBZ/fBZ*, and 1.51 ± 0.075 in *Wnt1Cre;fBZ/fBZ* mice (Fig. 9*F*). These results suggest that the effect of TrkB depletion on the development of the CF–PC synapse may be dissociated from an influence of BDNF on parallel fibre innervation during cerebellar development.

Discussion

The principal finding of the present study is that TrkB is necessary for the development of motor coordination and CF–PC synapses in the immature rodent cerebellum. Several lines of experimental evidence corroborate this finding. First, TrkB mutant mice displayed deficits in motor coordination and balance. Second, TrkB mutant mice had a higher proportion of Purkinje cells innervated by multiple climbing fibres at a developmental age when mono-innervation already prevailed in the wild-type cerebellar cortex. Third, in TrkB mutant mice, multiply innervated Purkinje cells display climbing fibre-evoked responses of similar amplitude, consistent with compromised competition. Fourth, parallel fibre transmission was normal in the TrkB mutant mice. Fifth, despite impaired pruning of supernumerary climbing fibres in the TrkB mutant mice, the climbing fibre terminals translocated unabated from the soma to the dendritic arbour of the Purkinje cell. These results, *in toto*, are consistent with pruning of climbing fibres being abnormal at the developing CF–PC synapse under conditions of TrkB depletion.

TrkB in the developing cerebellar cortex

In the present study, an important prerequisite demonstration was the neuroanatomical substrate for investigating the influence of TrkB on the development of the CF–PC synapse. Indeed, in agreement with earlier reports (Ringstedt *et al.* 1993; Gao *et al.* 1995; Carter *et al.* 2002; Dieni & Rees, 2002), our immunohistochemical observations point clearly to TrkB being expressed and widely distributed in the cerebellar cortex throughout postnatal development, particularly within the time frame when the electrophysiological studies were conducted in the present study. Other studies have reported a similar temporal and spatial pattern of distribution for BDNF and NT-4 (Timmusk *et al.* 1993; Castren *et al.* 1995; Li *et al.* 2001; Dieni & Rees, 2002). Overall, the presence of TrkB and BDNF in the postnatal cerebellar cortex places them in a favourable position to influence a number of landmark maturational events, including the shaping of the developing CF–PC synapse.

Aberrant neurotrophin expression and cerebellar dysfunction are arguably correlated with each other. Mice genetically depleted of BDNF or TrkB are ataxic (Schwartz *et al.* 1997; Rico *et al.* 2002). The stargazer mouse, with depleted levels of BDNF and TrkB signalling, are also ataxic (Qiao *et al.* 1996, 1998; Hashimoto *et al.* 1999). The results of the present study demonstrate that depletion of TrkB expression alone is sufficient to result in ataxia, and this may well be the point of convergence for many of the animal models in which BDNF expression is compromised and ataxia is observed.

It is noteworthy that the behavioural deficits as revealed by rotarod performance were as severe in the hypomorphic *fBZ/fBZ* mice as in the conditional knockout *Wnt1Cre;fBZ/fBZ* mice. Given that the *fBZ/fBZ* and the *Wnt1Cre;fBZ/fBZ* mice had similar climbing fibre innervation profiles, these results suggest that, although TrkB is expressed in the cerebellar cortex of the *fBZ/fBZ* mice, it may not be present at sufficient levels to affect proper regulation of the developing CF–PC synapse. An earlier study (Rico *et al.* 2002) reported that the neuronatomical phenotype of the *fBZ/fBZ* mice was often between those of the wild-type and the conditional *Wnt1Cre;fBZ/fBZ* knockout mice, resembling a 'heterozygous' situation. However, this did not appear to be the case in the present study. It may be that the behavioural tests employed in this study were not sufficiently sensitive to discriminate between any subtle differences in motor coordination between the *fBZ/fBZ* and *Wnt1Cre;fBZ/fBZ* mice.

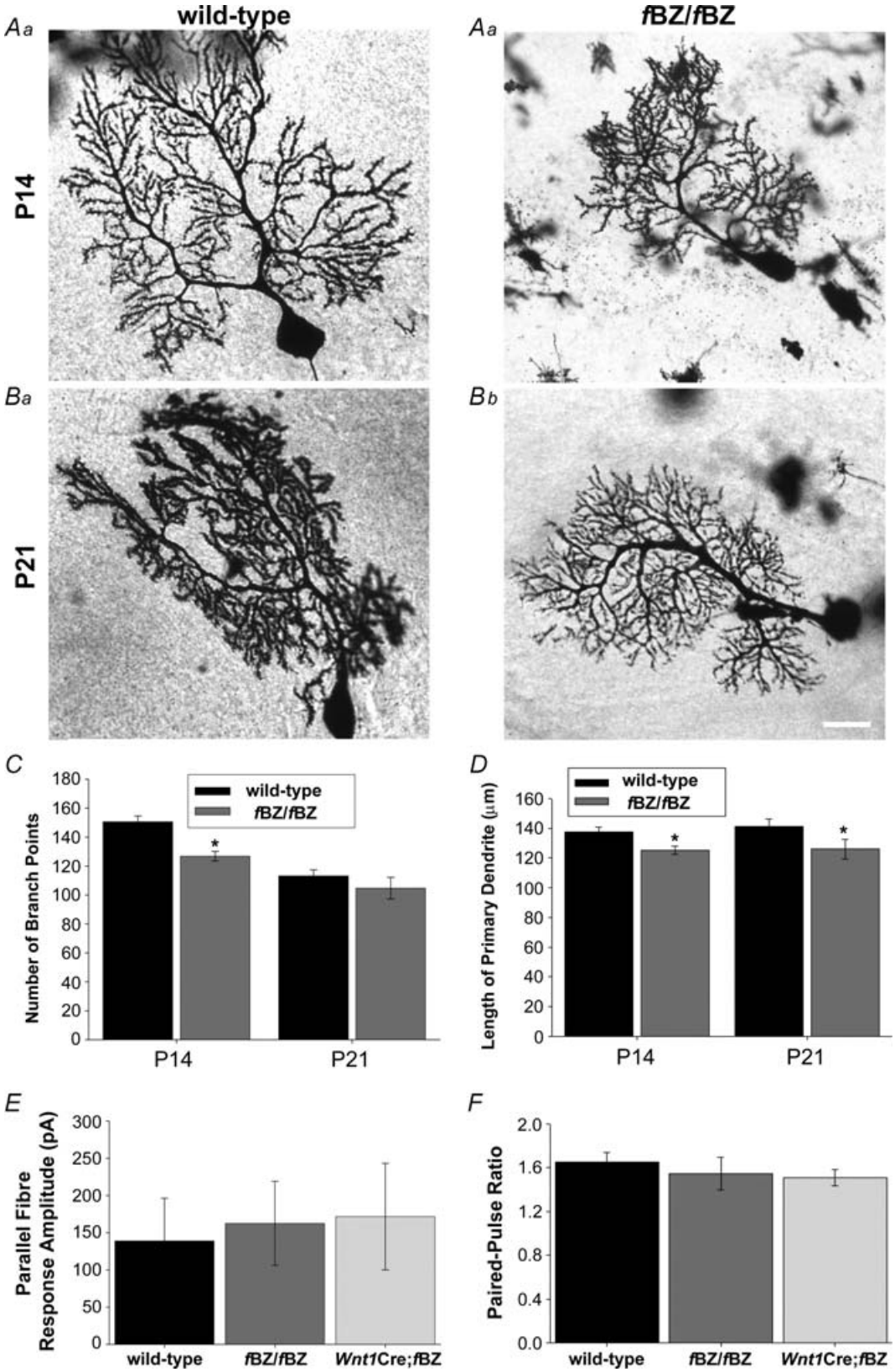

Figure 9. Parallel fibre synaptic transmission is normal at P20–24 in TrkB mutant mice despite an earlier delay in Purkinje cell dendritic development
A and *B*, examples of Golgi-impregnated Purkinje cells from wild-type (*a*) and *fBZ/fBZ* (*b*) at P14 (*A*) and P21 (*B*).

TrkB and synaptic pruning at the CF–PC synapse

A hallmark feature of synaptogenesis is the pruning of supernumerary contacts made at immature synaptic sites, and neurotrophins have been implicated in this process (Riva-Depaty *et al.* 1998; Sanes & Lichtman, 1999). The present study indicates that TrkB does not influence the initial innervation of Purkinje cells by climbing fibres, but plays a prominent role in regulating the regression of multiple climbing fibres innervating Purkinje cells in the developing cerebellum. Moreover, since elimination of supernumerary climbing fibres, albeit to more modest extents, was evident in the TrkB mutant mice, we propose that TrkB serves to modulate rather than control synaptic pruning. Such a modulatory role is consistent with many of its postulated modes of action in the developing and mature CNS (Shimada *et al.* 1998; Lom & Cohen-Cory, 1999; Tolwani *et al.* 2002; Wirth *et al.* 2003; Ji *et al.* 2005; Lush *et al.* 2005), including the modulation of granule cell maturation and migration in the developing cerebellar cortex (Gao *et al.* 1995; Segal *et al.* 1995; Schwartz *et al.* 1997; Bao *et al.* 1999; Borghesani *et al.* 2002).

A number of studies point to the development of the parallel fibre–Purkinje cell system and hypogranular cerebellum profoundly affecting the pruning of CF–PC synapses (Crepel *et al.* 1976, 1981; Puro & Woodward, 1978; Bravin *et al.* 1995; Kakizawa *et al.* 2000; Ichikawa *et al.* 2002; Scelfo & Strata, 2005; Hirai *et al.* 2005). BDNF knockout mice display both delayed dendritic development and impaired parallel fibre-Purkinje cell synaptic function (Carter *et al.* 2002). The implication here is that the action of TrkB on the developing CF–PC synapse is secondary to its primary influence on the development of parallel fibre–Purkinje cell synapses. However, it has been previously postulated that the early stages of climbing fibre pruning can occur independent of parallel fibre signalling (Crepel, 1982). Our study raises the possibility that factors other than the parallel fibre system may also modulate later stages of CF–PC synaptic development, insofar as normal parallel fibre synaptic transmission was demonstrable at a stage when multiple innervation by climbing fibres persisted. Rico *et al.* (2002) reported that Purkinje cell density and the granule cell–parallel fibre system were relatively normal in the TrkB mutant mice – cerebellar granule cells from both *fBZ/fBZ* and *Wnt1Cre*;*fBZ/fBZ* mice were comparable to those from wild-type mice in terms of morphology, size, parallel fibre diameter and density. We also found no differences in granule cell density between wild-type and TrkB mutant mice (data not shown). In addition, Rico *et al.* (2002) found decreased cross-sectional area in the molecular layer. While the precise cause is not known, this was attributed to decreased dendritic or axonal volume (Rico *et al.* 2002). The decreased branching of Purkinje cell dendrites we observed in the TrkB mutant mice is consistent with this notion.

Our results suggest that TrkB may play a developmental role in sorting out supernumerary climbing fibres innervating an immature Purkinje cell. This role does not appear to involve changes in presynaptic release mechanisms since paired-pulse ratio was unchanged in the TrkB mutant mice. However, under conditions in which TrkB expression is either diminished or absent, the contrast of strengths between the strong and weak innervating climbing fibres are obscured, resulting in a failure to establish a clear winning *vis-à-vis* a losing climbing fibre. This failure to discriminate between strengths of contending climbing fibres may underlie mechanistically the persistence of multiple climbing fibre innervation in the *fBZ/fBZ* and *Wnt1Cre*;*fBZ/fBZ* mice.

TrkB and translocation of CF–PC synapses

The culling of supernumerary climbing fibres innervating a Purkinje cell coincides temporally with the translocation of their terminals (Mason *et al.* 1990; Bravin *et al.* 1995; Overbeck & King, 1999; Morara *et al.* 2001; Scelfo *et al.* 2003; Sugihara, 2005). However, the signalling mechanisms underlying synaptic translocation and subsequent organization of climbing fibre terminals are not well understood. Deficits in pruning and translocation of climbing fibre contacts often occur concomitantly. Perturbations of the P/Q-type Ca^{2+} channel result in persistent innervation by multiple climbing fibres and failed translocation from the soma of the Purkinje cell (Miyazaki *et al.* 2004). Transgenic knockout of GluRδ2 or Cbln1 also results in persistent innervation by multiple climbing fibres but inappropriate translocation of climbing fibre terminals to distal dendritic extents of Purkinje cells usually designated as 'parallel fibre territory' (Hashimoto *et al.* 2001; Ichikawa *et al.* 2002; Hirai *et al.* 2005). Nonetheless, exceptions to this apparent association between persistence of multiple climbing fibre

Scale bar, 20 μm. *C*, total number of dendritic branch points. There are significantly fewer branches of *fBZ/fBZ* mice at P14 ($^*P < 0.001$ by one-way ANOVA), but not at P21 ($P = 0.079$ by one-way ANOVA). *D*, the length of the primary dendrite is shorter in *fBZ/fBZ* mice than wild-type mice at both P14 and P21 (P14 and P21: $^*P < 0.001$ by one-way ANOVA). *E*, average maximum amplitude of parallel fibre responses from wild-type, *fBZ/fBZ* and *Wnt1Cre*;*fBZ/fBZ* mice was comparable ($P = 0.930$ by one-way ANOVA). *F*, the ratio of parallel fibre-activated paired-pulse facilitation in Purkinje cells from wild-type, *fBZ/fBZ* and *Wnt1Cre*;*fBZ/fBZ* cerebellum was also comparable at P20–24 ($P = 0.632$ by one-way ANOVA).

innervation and aberrant translocation are evident in the literature (Bravin *et al.* 1995; Hashimoto *et al.* 2001). As a specific case in point, the climbing fibre terminals do not invade the 'parallel fibre territory' in mGluR1 knockout mice despite a deficit in the culling of climbing fibres (Kano *et al.* 1997; Ichise *et al.* 2000; Hashimoto *et al.* 2001). The results of our study corroborate this notion, as normal soma-to-dendrite translocation was demonstrated in electrophysiologically examined, Lucifer-yellow-filled Purkinje cells irrespective of whether a given Purkinje cell was multiply or singly innervated and whether TrkB was depleted.

Summary

Our results lead us to postulate the working hypothesis that, at the developing CF–PC synapse, separate processes regulate the culling of supernumerary climbing fibres and the topographical translocation of their terminals; TrkB appears to modulate synapse elimination, but not translocation. Within the grand scheme of synapse formation in the CNS, we propose that TrkB contributes to the moulding of nascent synapses by regulating axonal pruning.

References

Bao S, Chen L, Qiao X & Thompson RF (1999). Transgenic brain-derived neurotrophic factor modulates a developing cerebellar inhibitory synapse. *Learn Mem* **6**, 276–283.

Baquet ZC, Bickford PC & Jones KR (2005). Brain-derived neurotrophic factor is required for the establishment of the proper number of dopaminergic neurons in the substantia nigra pars compacta. *J Neurosci* **25**, 6251–6259.

Borghesani PR, Peyrin JM, Klein R, Rubin J, Carter AR, Schwartz PM, Luster A, Corfas G & Segal RA (2002). BDNF stimulates migration of cerebellar granule cells. *Development* **129**, 1435–1442.

Bravin M, Rossi F & Strata P (1995). Different climbing fibres innervate separate dendritic regions of the same Purkinje cell in hypogranular cerebellum. *J Comp Neurol* **357**, 395–407.

Cabelli RJ, Shelton DL, Segal RA & Shatz CJ (1997). Blockade of endogenous ligands of trkB inhibits formation of ocular dominance columns. *Neuron* **19**, 63–76.

Carter AR, Chen C, Schwartz PM & Segal RA (2002). Brain-derived neurotrophic factor modulates cerebellar plasticity and synaptic ultrastructure. *J Neurosci* **22**, 1316–1327.

Carter RJ, Lione LA, Humby T, Mangiarini L, Mahal A, Bates GP, Dunnett SB & Morton AJ (1999). Characterization of progressive motor deficits in mice transgenic for the human Huntington's disease mutation. *J Neurosci* **19**, 3248–3257.

Castren E, Thoenen H & Lindholm D (1995). Brain-derived neurotrophic factor messenger RNA is expressed in the septum, hypothalamus and in adrenergic brain stem nuclei of adult rat brain and is increased by osmotic stimulation in the paraventricular nucleus. *Neuroscience* **64**, 71–80.

Causing CG, Gloster A, Aloyz R, Bamji SX, Chang E, Fawcett J, Kuchel G & Miller FD (1997). Synaptic innervation density is regulated by neuron-derived BDNF. *Neuron* **18**, 257–267.

Cesa R & Strata P (2005). Axonal and synaptic remodeling in the mature cerebellar cortex. *Prog Brain Res* **148**, 45–56.

Crawley JN (1999). Behavioural phenotyping of transgenic and knockout mice: experimental design and evaluation of general health, sensory functions, motor abilities, and specific behavioural tests. *Brain Res* **835**, 18–26.

Crepel F (1971). Maturation of climbing fibre responses in the rat. *Brain Res* **35**, 272–276.

Crepel F (1982). Regression of functional synapses in the immature mammalian cerebellum. *Trends Neurosci* **5**, 266–269.

Crepel F, Delhaye-Bouchaud N & Dupont JL (1981). Fate of the multiple innervation of cerebellar Purkinje cells by climbing fibres in immature control, X-irradiated and hypothyroid rats. *Dev Brain Res* **1**, 59–71.

Crepel F, Delhaye-Bouchaud N & Legrand J (1976). Electrophysiological analysis of the circuitry and of the corticonuclear relationships in the agranular cerebellum of irradiated rats. *Arch Ital Biol* **114**, 49–74.

Danielian PS, Muccino D, Rowitch DH, Michael SK & McMahon AP (1998). Modification of gene activity in mouse embryos *in utero* by a tamoxifen-inducible form of Cre recombinase. *Curr Biol* **8**, 1323–1326.

Dieni S & Rees S (2002). Distribution of brain-derived neurotrophic factor and TrkB receptor proteins in the fetal and postnatal hippocampus and cerebellum of the guinea pig. *J Comp Neurol* **454**, 229–240.

Foster KA & Regehr WG (2004). Variance-mean analysis in the presence of a rapid antagonist indicates vesicle depletion underlies depression at the climbing fibre synapse. *Neuron* **43**, 119–131.

Fremeau RT Jr, Kam K, Qureshi T, Johnson J, Copenhagen DR, Storm-Mathisen J, Chaudhry FA, Nicoll RA & Edwards RH (2004). Vesicular glutamate transporters 1 and 2 target to functionally distinct synaptic release sites. *Science* **304**, 1815–1819.

Fremeau RT Jr, Troyer MD, Pahner I, Nygaard GO, Tran CH, Reimer RJ, Bellocchio EE, Fortin D, Storm-Mathisen J & Edwards RH (2001). The expression of vesicular glutamate transporters defines two classes of excitatory synapse. *Neuron* **31**, 247–260.

Gao WQ, Zheng JL & Karihaloo M (1995). Neurotrophin-4/5 (NT-4/5) and brain-derived neurotrophic factor (BDNF) act at later stages of cerebellar granule cell differentiation. *J Neurosci* **15**, 2656–2667.

Hashimoto K, Fukaya M, Qiao X, Sakimura K, Watanabe M & Kano M (1999). Impairment of AMPA receptor function in cerebellar granule cells of ataxic mutant mouse stargazer. *J Neurosci* **19**, 6027–6036.

Hashimoto K, Ichikawa R, Takechi H, Inoue Y, Aiba A, Sakimura K, Mishina M, Hashikawa T, Konnerth A, Watanabe M & Kano M (2001). Roles of glutamate receptor δ 2 subunit (GluRδ2) and metabotropic glutamate receptor subtype 1 (mGluR1) in climbing fibre synapse elimination during postnatal cerebellar development. *J Neurosci* **21**, 9701–9712.

Hashimoto K & Kano M (2003). Functional differentiation of multiple climbing fibre inputs during synapse elimination in the developing cerebellum. *Neuron* **38**, 785–796.

Hirai H, Pang Z, Bao D, Miyazaki T, Li L, Miura E, Parris J, Rong Y, Watanabe M, Yuzaki M & Morgan JI (2005). Cbln1 is essential for synaptic integrity and plasticity in the cerebellum. *Nat Neurosci* **8**, 1534–1541.

Hisano S, Sawada K, Kawano M, Kanemoto M, Xiong G, Mogi K, Sakata-Haga H, Takeda J, Fukui Y & Nogami H (2002). Expression of inorganic phosphate/vesicular glutamate transporters (BNPI/VGLUT1 and DNPI/VGLUT2) in the cerebellum and precerebellar nuclei of the rat. *Brain Res Mol Brain Res* **107**, 23–31.

Hu B, Nikolakopoulou AM & Cohen-Cory S (2005). BDNF stabilizes synapses and maintains the structural complexity of optic axons in vivo. *Development* **132**, 4285–4298.

Ichikawa R, Miyazaki T, Kano M, Hashikawa T, Tatsumi H, Sakimura K, Mishina M, Inoue Y & Watanabe M (2002). Distal extension of climbing fibre territory and multiple innervation caused by aberrant wiring to adjacent spiny branchlets in cerebellar Purkinje cells lacking glutamate receptor $\delta 2$. *J Neurosci* **22**, 8487–8503.

Ichise T, Kano M, Hashimoto K, Yanagihara D, Nakao K, Shigemoto R, Katsuki M & Aiba A (2000). mGluR1 in cerebellar Purkinje cells essential for long-term depression, synapse elimination, and motor coordination. *Science* **288**, 1832–1835.

Ji Y, Pang PT, Feng L & Lu B (2005). Cyclic AMP controls BDNF-induced TrkB phosphorylation and dendritic spine formation in mature hippocampal neurons. *Nat Neurosci* **8**, 164–172.

Jones BJ & Roberts DJ (1968). A rotarod suitable for quantitative measurements of motor incoordination in naive mice. *Naunyn Schmiedebergs Arch Exp Pathol Pharmakol* **259**, 211.

Kakizawa S, Yamasaki M, Watanabe M & Kano M (2000). Critical period for activity-dependent synapse elimination in developing cerebellum. *J Neurosci* **20**, 4954–4961.

Kaneko T & Fujiyama F (2002). Complementary distribution of vesicular glutamate transporters in the central nervous system. *Neurosci Res* **42**, 243–250.

Kano M, Hashimoto K, Kurihara H, Watanabe M, Inoue Y, Aiba A & Tonegawa S (1997). Persistent multiple climbing fiber innervation of cerebellar Purkinje cells in mice lacking mGluR1. *Neuron* **18**, 71–79.

Kano M, Hashimoto K, Watanabe M, Kurihara H, Offermanns S, Jiang H, Wu Y, Jun K, Shin HS, Inoue Y, Simon MI & Wu D (1998). Phospholipase C$\beta 4$ is specifically involved in climbing fibre synapse elimination in the developing cerebellum. *Proc Natl Acad Sci U S A* **95**, 15724–15729.

Kashiwabuchi N, Ikeda K, Araki K, Hirano T, Shibuki K, Takayama C, Inoue Y, Kutsuwada T, Yagi T & Kang Y (1995). Impairment of motor coordination, Purkinje cell synapse formation, and cerebellar long-term depression in GluR $\delta 2$ mutant mice. *Cell* **81**, 245–252.

Lalonde R (1987*a*). Motor abnormalities in weaver mutant mice. *Exp Brain Res* **65**, 479–481.

Lalonde R (1987*b*). Motor abnormalities in staggerer mutant mice. *Exp Brain Res* **68**, 417–420.

Li YX, Hashimoto T, Tokuyama W, Miyashita Y & Okuno H (2001). Spatiotemporal dynamics of brain-derived neurotrophic factor mRNA induction in the vestibulo-olivary network during vestibular compensation. *J Neurosci* **21**, 2738–2748.

Lom B & Cohen-Cory S (1999). Brain-derived neurotrophic factor differentially regulates retinal ganglion cell dendritic and axonal arborization *in vivo*. *J Neurosci* **19**, 9928–9938.

Lush ME, Ma L & Parada LF (2005). TrkB signalling regulates the developmental maturation of the somatosensory cortex. *Int J Dev Neurosci* **23**, 523–536.

Mariani J & Changeux JP (1981). Ontogenesis of olivocerebellar relationships. I. Studies by intracellular recordings of the multiple innervation of Purkinje cells by climbing fibres in the developing rat cerebellum. *J Neurosci* **1**, 696–702.

Mason CA, Christakos S & Catalano SM (1990). Early climbing fibre interactions with Purkinje cells in the postnatal mouse cerebellum. *J Comp Neurol* **297**, 77–90.

Miyazaki T, Fukaya M, Shimizu H & Watanabe M (2003). Subtype switching of vesicular glutamate transporters at parallel fibre–Purkinje cell synapses in developing mouse cerebellum. *Eur J Neurosci* **17**, 2563–2572.

Miyazaki T, Hashimoto K, Shin HS, Kano M & Watanabe M (2004). P/Q-type Ca^{2+} channel $\alpha 1A$ regulates synaptic competition on developing cerebellar Purkinje cells. *J Neurosci* **24**, 1734–1743.

Morara S, van der Want JJ, de Weerd H, Provini L & Rosina A (2001). Ultrastructural analysis of climbing fibre-Purkinje cell synaptogenesis in the rat cerebellum. *Neuroscience* **108**, 655–671.

Nishiyama H & Linden DJ (2004). Differential maturation of climbing fibre innervation in cerebellar vermis. *J Neurosci* **24**, 3926–3932.

Offermanns S, Hashimoto K, Watanabe M, Sun W, Kurihara H, Thompson RF, Inoue Y, Kano M & Simon MI (1997). Impaired motor coordination and persistent multiple climbing fibre innervation of cerebellar Purkinje cells in mice lacking Gαq. *Proc Natl Acad Sci U S A* **94**, 14089–14094.

Overbeck TL & King JS (1999). Developmental expression of corticotropin-releasing factor in the postnatal murine cerebellum. *Brain Res Dev Brain Res* **115**, 145–159.

Puro DG & Woodward DJ (1977). Maturation of evoked climbing fibre input to rat cerebellar purkinje cells (I). *Exp Brain Res* **28**, 85–100.

Puro DG & Woodward DJ (1978). Physiological properties of afferents and synaptic reorganization in the rat cerebellum degranulated by postnatal X-irradiation. *J Neurobiol* **9**, 195–215.

Qiao X, Chen L, Gao H, Bao S, Hefti F, Thompson RF & Knusel B (1998). Cerebellar brain-derived neurotrophic factor-TrkB defect associated with impairment of eyeblink conditioning in Stargazer mutant mice. *J Neurosci* **18**, 6990–6999.

Qiao X, Hefti F, Knusel B & Noebels JL (1996). Selective failure of brain-derived neurotrophic factor mRNA expression in the cerebellum of stargazer, a mutant mouse with ataxia. *J Neurosci* **16**, 640–648.

Ribar TJ, Rodriguiz RM, Khiroug L, Wetsel WC, Augustine GJ & Means AR (2000). Cerebellar defects in Ca^{2+}/calmodulin kinase IV-deficient mice. *J Neurosci* **20**, RC107.

Rico B, Xu B & Reichardt LF (2002). TrkB receptor signalling is required for establishment of GABAergic synapses in the cerebellum. *Nat Neurosci* **5**, 225–233.

Ringstedt T, Lagercrantz H & Persson H (1993). Expression of members of the trk family in the developing postnatal rat brain. *Brain Res Dev Brain Res* **72**, 119–131.

Riva-Depaty I, Dubreuil YL, Mariani J & Delhaye-Bouchaud N (1998). Eradication of cerebellar granular cells alters the developmental expression of trk receptors in the rat inferior olive. *Int J Dev Neurosci* **16**, 49–62.

Sanes JR & Lichtman JW (1999). Development of the vertebrate neuromuscular junction. *Annu Rev Neurosci* **22**, 389–442.

Scelfo B & Strata P (2005). Correlation between multiple climbing fibre regression and parallel fibre response development in the postnatal mouse cerebellum. *Eur J Neurosci* **21**, 971–978.

Scelfo B, Strata P & Knopfel T (2003). Sodium imaging of climbing fibre innervation fields in developing mouse Purkinje cells. *J Neurophysiol* **89**, 2555–2563.

Schwartz PM, Borghesani PR, Levy RL, Pomeroy SL & Segal RA (1997). Abnormal cerebellar development and foliation in BDNF–/– mice reveals a role for neurotrophins in CNS patterning. *Neuron* **19**, 269–281.

Segal RA, Pomeroy SL & Stiles CD (1995). Axonal growth and fasciculation linked to differential expression of BDNF and NT3 receptors in developing cerebellar granule cells. *J Neurosci* **15**, 4970–4981.

Shimada A, Mason CA & Morrison ME (1998). TrkB signalling modulates spine density and morphology independent of dendrite structure in cultured neonatal Purkinje cells. *J Neurosci* **18**, 8559–8570.

Silver RA, Momiyama A & Cull-Candy SG (1998). Locus of frequency-dependent depression identified with multiple-probability fluctuation analysis at rat climbing fibre–Purkinje cell synapses. *J Physiol* **510**, 881–902.

Stevens CF & Wang Y (1995). Facilitation and depression at single central synapses. *Neuron* **14**, 795–802.

Sugihara I (2005). Microzonal projection and climbing fibre remodeling in single olivocerebellar axons of newborn rats at postnatal days 4–7. *J Comp Neurol* **487**, 93–106.

Timmusk T, Belluardo N, Metsis M & Persson H (1993). Widespread and developmentally regulated expression of neurotrophin-4 mRNA in rat brain and peripheral tissues. *Eur J Neurosci* **5**, 605–613.

Tolwani RJ, Buckmaster PS, Varma S, Cosgaya JM, Wu Y, Suri C & Shooter EM (2002). BDNF overexpression increases dendrite complexity in hippocampal dentate gyrus. *Neuroscience* **114**, 795–805.

Wirth MJ, Brun A, Grabert J, Patz S & Wahle P (2003). Accelerated dendritic development of rat cortical pyramidal cells and interneurons after biolistic transfection with BDNF and NT4/5. *Development* **130**, 5827–5838.

Xu B, Gottschalk W, Chow A, Wilson RI, Schnell E, Zang K, Wang D, Nicoll RA, Lu B & Reichardt LF (2000). The role of brain-derived neurotrophic factor receptors in the mature hippocampus: modulation of long-term potentiation through a presynaptic mechanism involving TrkB. *J Neurosci* **20**, 6888–6897.

Acknowledgements

We thank Dr Robert Maue for critically reading the manuscript. This work was supported by PHS F31 NS053069 (E.J.) and RO1 MH069826 (H.H.Y.).